Resonantly excited cascade x-ray emission from La

A. Moewes and R. G. Wilks
Department of Physics and Engineering Physics, University of Saskatchewan, 116 Science Place, Saskatoon, Saskatchewan S7N 5E2, Canada

A. G. Kochur
Rostov State University of Transport Communications, Rostov-na-Donu 344038, Russia

E. Z. Kurmaev
Institute of Metal Physics, Russian Academy of Sciences-Ural Division, 620219 Yekaterinburg GSP-170, Russia
(Received 6 April 2004; revised manuscript received 23 June 2005; published 22 August 2005)

We are monitoring the intensity of the La $5p$-$4d$ emission for La metal while scanning across the deeper lying $3d$-$4f$ photoexcitation resonances of the same atom. A strong resonant enhancement in the integral intensity of the La $5p$-$4d$ fluorescence emission is observed, which is due to cascading decay of the resonantly excited $3d^9 4f^{+1}$ configuration. The corresponding emission spectrum features a complex satellite structure reflecting the multitude of transitions taking place in a variety of multi-vacancy configurations created by the cascade. We calculate the probability of $5p \rightarrow 4d$ emission produced by the cascading decay and then take into account self-absorption of the emitted photons. This model provides good agreement with the experimental results. The number of $4d$ vacancies increases immensely due to electronic cascades. We also observe an enhanced integral intensity in the $5p$-$4d$ fluorescence compared to our calculations, which we attribute to intra-atomic resonance processes.

DOI: 10.1103/PhysRevB.72.075129 PACS number(s): 78.70.En, 78.70.Dm, 32.80.Fb

I. INTRODUCTION

A variety of phenomena are observed when resonantly exciting soft x-ray emission spectra. When the energy of the incoming photons is tuned through the absorption thresholds of the emitting atoms, the corresponding soft x-ray emission spectra demonstrate numerous features that disperse strongly with changes in the excitation energy.[1,2] In this resonant case, the absorption and emission behavior is described as a single second-order optical process.

This behavior means in particular that any process observable via photoemission will also generally be detectable as a secondary process through x-ray fluorescence, although the fluorescence detection may be experimentally hampered by inherently low quantum yields and intrinsically small spectrometer efficiency.

In the present paper we first analyze the effects that arise in the fluorescence spectra of selected emitting atoms when the excitation energy is scanned through energetically deeper lying thresholds of the *same* atom. We are monitoring the dependence on excitation energy of the (partial) La $N_{4,5}$ soft x-ray emission ($5p_{1/2,3/2} \rightarrow 4d_{3/2,5/2}$ transitions located at 77 to 90 eV) for La metal while exciting through the much deeper lying La $M_{4,5}$ thresholds ($3d \rightarrow 4f$ transition at 824 to 861 eV). The question is: How is fluorescent decay in a certain channel (La $N_{4,5}$) affected when exciting through a deeper lying threshold ($M_{4,5}$) of the same atom? To our knowledge, this fundamentally important question has, surprisingly, not yet been studied in the literature for solid samples. The only similar experiments concerned atomic $5p$-$4d$ fluorescence spectra of gaseous Xe excited at the $3d$ threshold.[3–5]

Analysis of this resonant effect is generally important to the fluorescence community, as well as to the absorption spectroscopy community, since it requires *quantitative* absorption measurements in order to properly account for self-absorption of the emitted photons.

Krause *et al.*[6] have measured the partial photoemission cross section for Mn $3d$ electrons and found a resonant enhancement in $3d$ and $4s$ photoemission when the excitation energy passes through the lower-lying $3p$ thresholds. More specifically, the measurements of the partial $3d$ cross section agreed with many-body calculations by Garvin *et al.*,[7] the $4s$ channel was found to be larger in Krause's experiment than in Garvin's theory. The discrepancy was generally ascribed to "resonances due to the excitation of a $3d$ electron and two electron-excitations."[6]

We note that the experimental setup is very similar to that used for multiatom resonant effects.[8] This effect was believed to occur (for MnO) when the excitation energy is tuned to a low-lying core-level absorption edge of one atom (Mn $2p$) while monitoring the fluorescence decay from a higher lying transition of another neighboring atom (O $2p \rightarrow 1s$). It was suggested that enhanced fluorescence emission from the O $1s$ core level involves a resonance with deeper lying Mn $2p$ levels. Contrary to this, it was found that such an effect (in fluorescence) either does not exist at all, or is much smaller ($<3\%$) than previously suggested.[9] It was later discovered that the suspected multiatom resonances in photoemission could largely be attributed to nonlinearities in the detector.[10,11] We note that when resonant enhancement effects are being discussed, one has to carefully consider which thresholds ($3p$,$3d$) are probed and which processes (fluorescence, photo electrons or Auger electrons) are being used to probe them.

In this paper we observe the photon emission that is the result of cascade mechanisms: $5p$-$4d$ photons are emitted from $4d$-vacancy states that are produced during the cascading decay of innershell vacancies that are triggered by photoionization near the $3d$ threshold. A number of studies have been devoted to both experimental and theoretical examinations of soft x-ray photoabsorption in the vicinity of the $3d$-ionization thresholds in metallic lanthanum and in lanthanum compounds.[12–14] The first complete comparison between theoretical and synchrotron-based $3d$-$4f$ absorption spectra for all Lanthanides was presented by Thole *et al.*[15] Photoabsorption in this region was found to be dominated by $3d$-$4f$ excitation, which can be described using an atomic model because the $4f$ orbital in La is well localized and its atomic character is preserved. We also use the isolated-atom approximation for the calculation of both photoabsorption and cascade-produced $5p$-$4d$ emission. Resonant La $5p \rightarrow 4d$ and $4f \rightarrow 4d$ emission spectra are studied in detail in Ref. 16.

II. EXPERIMENTAL DETAILS

The measurements were performed at Beamline 8.0.1 of the Advanced Light Source at Lawrence Berkeley National Laboratory. The undulator radiation is dispersed by a spherical-grating monochromator[17] and delivered to the sample, where a spherical-grating spectrometer in Rowland geometry analyzes the energy of the radiation emitted by the sample. In the present experimental geometry, the angle between the incident beam and the spectrometer axis is fixed at 90° and the plane of polarization is in the plane of incidence. The emission angle is therefore equal to 90° minus the angle of incidence. Both angles are measured with respect to the sample surface. The absorption spectra are measured in the sample current mode [total electron yield (TEY)]. All absorption and partial fluorescence yield (PFY) spectra are normalized to the number of photons falling onto the sample, which is monitored by recording the current produced when a highly transparent gold mesh in front of the sample is illuminated by the incoming soft x-rays. The sample was a piece of La metal, and its surface was cleaned in ultrahigh vacuum (3×10^{-9} Torr) prior to the measurements by scraping it with a diamond file. All of the measurements were performed at room temperature. All of the experimental curves are displayed as measured, without broadening or smoothing of data.

III. MEASUREMENTS

Figure 1 shows the partial fluorescence yield (PFY) of the La $5p \rightarrow 4d$ emission (centered at 83.5 eV) that was obtained when scanning the excitation energy through the La $3d$-$4f$ threshold (824 to 861 eV). The detector window was set such that it could integrally measure all photons emitted between 77 and 90 eV; a range which covers the broad features labeled *A* (top inset) that mainly stem from $4d^9 5p^6 4f^{+1} \rightarrow 4d^{10} 5p^5 4f^{+1}$ transitions. The total energy-dependent count rate in the detector window is displayed in Fig. 1 as the partial $5p \rightarrow 4d$ fluorescence yield. The detector window is

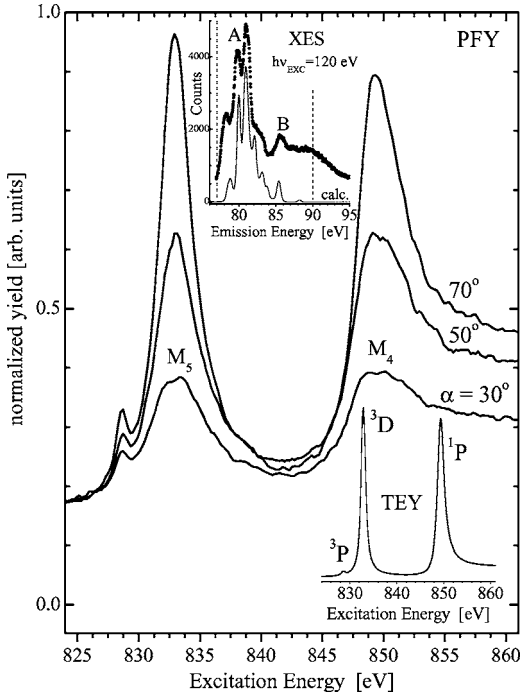

FIG. 1. Partial ($5p \rightarrow 4d$) fluorescence yields (PFY) of metallic La for three different incidence angles α (measured to the sample surface). The PFY spectra are normalized to the same count rate at 824 eV. The top inset displays the soft x-ray emission spectrum excited at 120 eV, which corresponds to the N_4 ($4d$-$4f$) resonance ($h\nu_{exc}=120$ eV) as a dotted line. The solid curve below shows an atomic calculation using the COWAN code (Ref. 25) of the fluorescence spectrum taking into account all possible decays from intermediate state configurations $4d^9 4f^1$ and $4d^9 4f^0$ taken from Ref. 16. The dashed vertical lines mark the detector window (77 to 90 eV) used for the partial fluorescence yield measurements. The bottom inset shows the $3d$-$4f$ absorption spectrum measured in total electron yield (TEY) mode including the terms of the excited state (notation $^{2S+1}$L). PFY and TEY spectra were measured simultaneously with the same experimental resolution.

schematically shown by the two vertical lines in the top inset of Fig. 1.

Figure 1 displays the partial fluorescence yield curves measured at three different angles of incidence. For smaller angles of incidence the spectral contrast decreases due to stronger self-absorption, which can be explained quantitatively by the angular dependence discussed below [Eq. (2)]

The $5p \rightarrow 4d$ fluorescence intensity is directly proportional to the number of $4d$ holes that are present at a given time. The inset of Fig. 2 shows the calculated $4d$-, $4s$-, $4p$-, and $3d$-$4f$ cross sections. Although the number of $4d$ holes created *directly* by the incoming photons is nearly constant through the $3d$-$4f$ threshold (as well as the number of $4p$ and $4s$ holes), an increase in the $5p \rightarrow 4d$ fluorescence is observed upon creation of a $3d$ hole. It is shown below that the increase in the partial fluorescence yield spectra is due to an increase in $4d$ holes that are created through secondary cascade processes that follow the creation of $3d$ holes, and which subsequently decay partially via $5p$-$4d$ fluorescence. The shape of the PFY spectra, therefore, resembles the shape of the $3d$-$4f$ absorption spectrum.

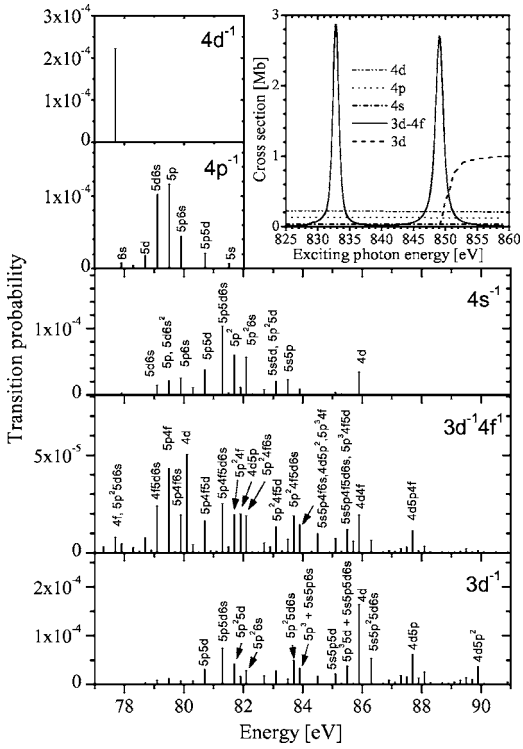

FIG. 2. Transition probabilities and energy positions of the principal radiative decay channels for atomic lanthanum upon decay of various intermediate states (ionization of $3d$, $4s$, $4p$, and $4d$ shell plus upon $3d$-$4f$ photoexcitation). The most intense transitions are labeled by specifying the spectator vacancies in whose presence the $5p \rightarrow 4d$ transition takes place. The inset shows the partial photoionization (of $4d$, $4s$, and $4p$) and photoexcitation ($3d$-$4f$) cross sections of atomic lanthanum through the $3d$-$4f$ thresholds.

The inset in Fig. 2 shows that the $5p$-$4d$ fluorescence evolves as follows: When exciting at the $M_{4,5}$ thresholds, the PFY is dominated by cascades starting from the $3d^{-1}4f^{+1}$ configuration. For other, off-resonance excitation energies, the $4d$ photoabsorption process is dominant, and the normal $5p$-$4d$ emission plays an important role.

IV. CALCULATIONS

In this section the methods used for calculating the PFY spectra are outlined. When exciting at photon energy ε, the $5p \rightarrow 4d$ fluorescence emission is registered by a detector which is centered at energy position E, and which is accepting photons that fall within an energy range that corresponds to the detector window ΔE. The partial $5p \rightarrow 4d$ fluorescence yield is calculated using the expression

$$\mathrm{PFY}(\varepsilon, E, \Delta E) \propto \sum_j \sigma_j(\varepsilon) P_j(E, \Delta E), \qquad (1)$$

where the index j denotes the photoionization ($4d$, $4p$, $4s$, $3d$) and photoexcitation ($3d$-$4f$), σ_j is the corresponding photoionization or photoexcitation cross section, and $P_j(E, \Delta E)$ is the probability of detecting a photon in the energy interval ΔE upon the decay of the $4d^{-1}$, $4p^{-1}$, $4s^{-1}$, $3d^{-1}$, and $3d^{-1}4f^{+1}$ states.

The parameters that are used to describe the observed emission intensities are photoionization and photoexcitation cross-sections and the energy positions of the $5p \rightarrow 4d$ emission features. Aside from the simplest case—emission from the intermediate state with a directly created $4d$ hole ($4d^{-1}$)—all decays starting from the $4p^{-1}$, $4s^{-1}$, $3d^{-1}$, and $3d^{-1}4f$ states include cascade effects.

Any atomic innershell vacancy results in a usually short-lived excited state that is liable to decay. Since the neighboring sub-shells are usually the most likely ones to participate in transitions, the decay of inner-shell vacancies can involve complex multistep cascades of consecutive transitions.[18]

Since every radiationless transition in a cascade leads to the ejection of an electron, the decay cascade creates a variety of intermediate multivacancy configurations. Consequently, low-energy emission spectra, such as the $5p \rightarrow 4d$ emission presented here, display complex multicomponent satellite structures caused by the decay of the states produced through $4p$, $4s$, and $3d$ photoionization and by $3d$-$4f$ photoexcitation.

The cascade spectra are calculated via straightforward construction of the relaxation branches using methods described in detail elsewhere.[19,20] The principal features of the theoretical model that is employed are as follows.

Branching ratios for each initial or intermediate configuration of the deexcitation tree are calculated using radiative and non-radiative partial widths obtained using a one-electron approximation. All radiative and non-radiative decay paths that are energetically possible are considered for every intermediate configuration in a cascade decay. Over 2000 different configurations are encountered for the most complex cascades. Configuration energies are calculated using Pauli-Fock approximation.

We have used the isolated-atom approximation for the calculation of both the cross sections $\sigma_j(\varepsilon)$ and the emission probabilities $P_j(E, \Delta E)$. The calculations are performed for the neutral configuration of the La atom $5d^1 6s^2$. Although the outermost $5d$ and $6s$ electrons form the valence band in the solid and are therefore delocalized, they are still present within the lattice and the electronic charge within the sphere of each individual atom is effectively zero. In this approximation one can consider $5d$ and $6s$ electrons as providing an approximate representation of the valence band.

Simulations of the spectra produced by the decay of the ionized $3d^{-1}$, $4d^{-1}$, $4p^{-1}$, $4s^{-1}$ states and the resonantly excited $3d^{-1}4f^{+1}$ states are shown in Fig. 2. The height of each bar in Fig. 2 reflects the probability of detecting a photon in a particular energy channel upon creation of the corresponding innershell vacancy. The most relevant transitions are labeled by listing the additional vacancies in whose presence transitions are taking place. Calculated atomic spectra in Fig. 2 are shifted by 9 eV to lower energies so that they may be compared to the experiment on metal. The shift of emission spectra to lower energies when going from free atoms to metals is due to extra-atomic relaxation. Relaxation is larger for the initial-vacancy states than for the final-vacancy ones, which leads to lower photon energies in metals.

We note that the spectra from the decay of $4p^{-1}$, $4s^{-1}$, $3d^{-1}$, and $3d^{-1}4f^{+1}$ are due to satellite emission exclusively and have complex multicomponent structures. Since the ex-

citation energies for photoionization of $4d$, $4p$, and $4s$ shells are far above threshold, the corresponding cross-sections are calculated using the frozen core approximation.

The $3d$-$4f$ photoexcitation cross section is calculated using the intermediate coupling scheme. The natural width of the components arising from the $3d_{5/2}{}^{-1}4f^{+1}$ states $\Gamma(3d_{5/2}{}^{-1}4f^{+1})$ is 0.636 eV and is calculated by considering all possible Auger decay paths for the $3d_{5/2}{}^{-1}4f^{+1}$ states. Coster-Kronig processes, primarily the $M_{3/2}M_{5/2}N_{67}$ (Ref. 21) process, cause the width of the $3d_{3/2}{}^{-1}4f^{+1}$ components to be larger than that of the $3d_{5/2}{}^{-1}4f^{+1}$. The ratio of the areas beneath the calculated peaks ($\sigma_{3/2}/\sigma_{5/2}=1.24$) closely resembles the experimental results, and so the widths of the $3d_{3/2}{}^{-1}4f^{+1}$ components were adjusted such that they reproduce the shape of the experimental photoexcitation cross section. The fitted value is $\Gamma(3d_{3/2}{}^{-1}4f^{+1})=1.1$ eV, in agreement with the results of Ref. 21, where, based on comparison between $4f$-$3d$ emission and $3d$-$4f$ absorption, the ratio $\Gamma(3d_{3/2}{}^{-1}4f^{+1})/\Gamma(3d_{5/2}{}^{-1}4f^{+1})$ in La was found to be 1.6. As for the absolute value of $\Gamma(3d_{5/2}{}^{-1}4f^{+1})$, our result (0.636 eV) is similar to the atomic calculation of McGuire (Ref. 22) (0.73 eV). Other authors report both much larger[21] (1.6 eV) and smaller[15] (0.4 eV) values. It should be noted that the experimental La metal photoabsorption spectrum taken in the TEY mode with 0.4 eV monochromator resolution in Ref. 15 has a full width at half maximum (FWHM) of about 1.5 eV for the $M_{5/2}$ line. The authors of Ref. 15 argued that, due to the loss processes associated with x-ray absorption length, electron escape depth, and experimental geometry, the experimental photoabsorption spectrum lines could become noticeably wider as compared with natural-width lines. An experiment on La in gas phase would show if the loss processes in a solid sample would produce such a strong effect. In order to account for the experimental resolution, the calculated natural profile of the $3d$-$4f$ photoexcitation was convoluted with a Gaussian curve of width 1.35 eV.

Calculated photoionization and photoexcitation cross sections are shown in the inset in Fig. 2. We note that the calculated $3d$-ionization cross section is larger than in the experimental TEY spectrum (inset in Fig. 1). We attribute this difference to the use of the atomic model, with the term $P_{3d\text{-}4f}(E,\Delta E)$ in Eq. (1) being largely responsible for the overestimation. Our calculated $3d$-excitation/$3d$-ionization ratio for La is similar to that which has been experimentally determined for the gas phase of the neighboring atom Ba.[23]

V. CALCULATION OF SELF-ABSORPTION AND DISCUSSION

In order to correct the calculated partial fluorescence yield for self-absorption of the emitted (and incident) radiation, the following expression[9] was used:

$$\frac{dN_{\mathrm{PFY}}}{N_0\, d\Omega} \propto \sum_{i,j} \omega_{i,j} \frac{1}{\mu + \mu_{i,j} \tan \alpha}. \tag{2}$$

In this equation dN_{PFY} denotes the number of photons emitted by the sample into the solid angle $d\Omega$. N_0 is the number of photons falling on the sample and μ stands for the total photoabsorption coefficient of the incoming photons. The indices i,j describe the summation over all existing core holes i and their possible decay channels j. The quantity $\mu_{i,j}$ is the absorption coefficient for the fluorescence radiation resulting from the transition from level j to i, that occurs with a fluorescence yield $\omega_{i,j}$.

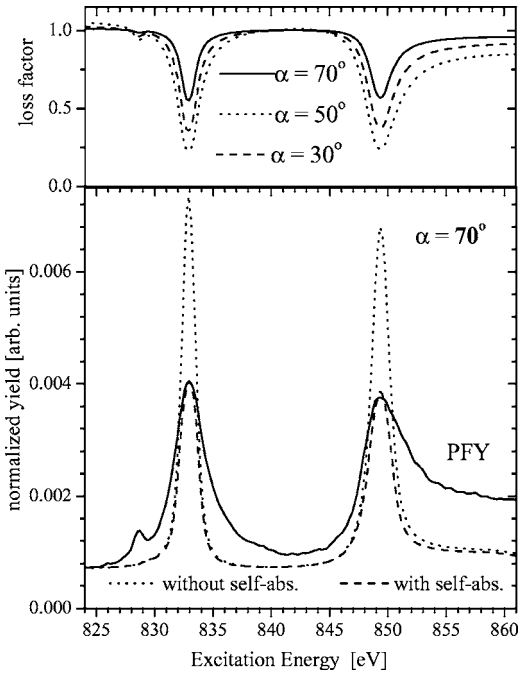

FIG. 3. Measured partial fluorescence yield (PFY) and calculations without correction for self-absorption (dotted line) and with correction for self-absorption. The upper panel shows the angular dependence of the correction factors for self-absorption losses for the three different incidence angles.

The number of fluorescence photons created in the present detector window was calculated using Eq. (1), and this spectrum was then corrected for self-absorption employing Eq. (2). The self-absorption of the emitted fluorescence (and incident) radiation depends entirely on the ratio $1/(\mu + \mu_{i,j} \tan \alpha)$. Equation (2) assumes that the sample is thick compared to the penetration depth of the exciting radiation, and it obviously also neglects Compton processes. Reflection of the incoming and outgoing radiation at the sample interface is neglected as well, which is a reasonable omission since the calculated reflectivity (for $\alpha=30°$) at the interface is smaller than 4×10^{-6} and 7×10^{-4} for incoming and outgoing photons, respectively.[24]

Figure 3 shows quantitatively the effect of self-absorption and the two steps of our calculation. The uncorrected partial fluorescence yield that was calculated using Eq. (1) is shown as a dotted line in the main window of the figure. In order to account for self-absorption of the emitted radiation, this curve is then multiplied by a self-absorption loss factor derived from Eq. (2), which is shown for three angles of incidence in the inset of Fig. 3. The product of the calculated partial fluorescence yield and the self-absorption loss factor corresponding to incidence angle $\alpha=70°$ is shown as the dashed line in the main window of Fig. 3. The ratio of the intensity of the resonant peak to the prethreshold background

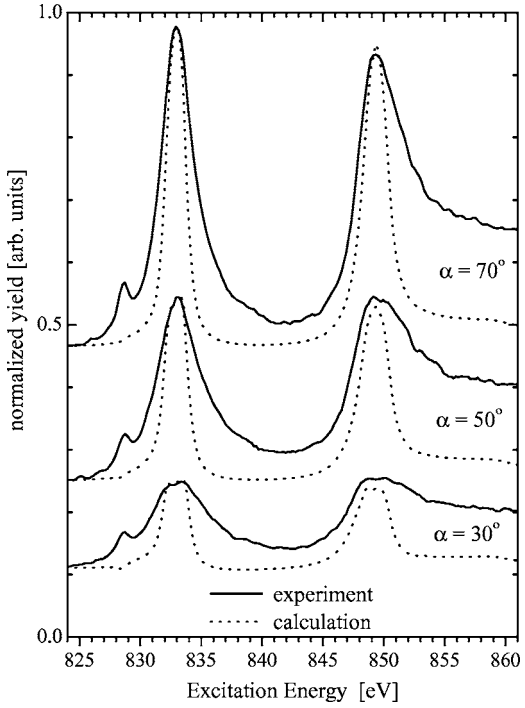

FIG. 4. Measured (solid line) and calculated (dashed line) partial fluorescence (La $5p \rightarrow 4d$) intensity for excitation energies through the $3d$-$4f$ thresholds for three different incidence angles (to the sample surface). The spectra are offset in the y direction for clarification.

level in the corrected theoretical PFY closely resembles that of the measured PFY curve that is displayed as a solid line in the main window of Fig. 3. It can be seen in the inset of Fig. 3 that, in the present scenario, self-absorption reduces the fluorescence radiation more strongly for more grazing angles of incidence.

In Fig. 4 we compare the PFY measurements (as displayed in Fig. 1) with our model calculations for the partial fluorescence yields. The calculated spectra match the measured curves well in terms of the contrast in the curves. We note that for all angles of incidence the *integral* fluorescence yield of the measured data is larger than that of the calculated spectrum.

In order to discuss the validity of the model applied, it is important to note that two parameters are essential for a correct estimation of the self-absorption and therefore for the calculation of the PFY: (1) It is necessary to measure the correct (relative) total absorption spectrum $\mu(E)$ and (2) to obtain the correct *ratio* of absorption coefficients $\mu_{i,j}$ to $\mu(E)$ as required in Eq. (2). The (relative) absorption coefficient $\mu(E)$ is determined by our measurement (as shown in the inset of Fig. 1).

It is evident from Eq. (2) that the contrast obtained in the measured absorption $\mu(E)$ determines, to a large degree, how well (in terms of the contrast of the PFY curves) the experimental results will be reproduced by the model. The crucial parameter for the comparison between calculation and measurement is, therefore, the peak-to-background ratio obtained in the measured $3d$-$4f$ absorption spectrum. It is, in our view, necessary to use the same instrumental resolving power for the exciting radiation when obtaining partial fluorescence and electron yield absorption spectra. Any attempt to broaden the experimental absorption data would add uncertainty to the absorption spectrum in terms of the peak-to-background ratio. Increasing the resolving power in the TEY spectrum will increase its peak-to-background ratio, and will lead to a too-strong correction for self-absorption. This change in the peak-to-background ratio would ultimately result in a smaller contrast in the calculated PFY curve. For this reason the TEY absorption and the partial fluorescence emission spectra were measured simultaneously. Due to the inherently low fluorescence yield count rates a moderate resolution of $E/\Delta E \approx 630$ was chosen, although the strong signal provided by the absorption measurement would have allowed for absorption spectra to be obtained at maximum resolving power ($E/\Delta E \approx 5000$).

In order to determine the ratio $\mu_{i,j}/\mu$, a second absorption spectrum has been measured that extends across both the threshold of the fluorescence emission ($5p \rightarrow 4d$) and the threshold of the excitation ($3d \rightarrow 4f$). The ratio was determined experimentally to be $\mu_{i,j}(81\ \text{eV}) = 10\mu(825\ \text{eV})$ for La. For comparison, the values obtained from Henke's atomic scattering factors[24] are 2.9 for La and 6.6 for La_2O_3. This disparity indicates that oxide layers are still present on the measured sample. A decrease in the ratio of μ_{ij} to μ would lead to a decrease in the height of the calculated fluorescence yields (of up to 50% for $\alpha = 70°$ if one would use the Henke value of 2.9 for La). The difficulty remains in accurately measuring a quantitative absorption spectrum from a chemically reactive sample (La) over an extended energy range. The common solution to this problem—performing transmission measurements of a thin film prepared *in situ*—is not practical in our case for the following two reasons: (1) For a sample that is not much thicker than the photon attenuation length, the sample thickness will introduce another parameter into Eq. (2) and (2) both spectra, PFY and XAS, have to be taken from the same sample; preferably simultaneously as in our measurements.

The FWHM of the measured spectra in Fig. 4 are larger than those of the calculated spectra. Although it is presently not clear what this effect is due to, the following three possibilities can be ruled out (1) An instrumental effect; since we control and measure the resolution of both the monochromator and spectrometer. (2) A reduction in the intensity of the incoming radiation due to reflection of the emitted photons at the vacuum/sample interface cannot lead to a dramatic reduction of emitted radiation since the reflection coefficients are too small as discussed above. (3) One can exclude that the difference in measured and calculated energy width of the PFY spectra is due to severe mistakes in theoretical level widths. The shape of the theoretical PFY spectrum is determined by the $3d$-$4f$ cross section only, and the widths of the peaks of calculated PFY and experimental TEY absorption spectra compare well. The width of the $4d$ hole can only affect the profile of the $4d$-$5p$ emission spectrum, not the PFY spectrum, since in our experiment the photons are detected in a very large energy window.

Finally, we compare the areas under the calculated and measured partial fluorescence yield curves. These areas are proportional to the total number of $5p$-$4d$ fluorescence pho-

tons. They were determined by integrating over the PFY curves after subtracting the prethreshold background signal, and the ratio of the measured to the calculated number of photons was found to have an average value of 2.4 (2.2 for $\alpha=70°$, 2.5 for $\alpha=50°$, and 2.5 for $\alpha=30°$). This ratio of 2.4 would increase to 4.2 if the smaller Henke value of 2.9 for $\mu_{i,j}(81\ \text{eV})/\mu(825\ \text{eV})$ was used and the trends would be the same but the effect would be quantitatively stronger.

The larger number of La $4d$ holes found in the PFY measurement (compared to the calculations) is interpreted as being due to mechanisms *other than cascades*. The exact mechanism that leads to the increase remains unclear. It is possible that the additional resonant interaction could be associated with electron correlation effects that are not included in our model. We also note that the count rate of the calculated spectra well above the threshold ($E>852$ eV) decreases to a lower value than observed in the measured spectra. This discrepancy must be caused by an underestimation of the calculated (atomic) $5p$-$4d$ emission probability involving cascades arising from an initial $3d$ vacancy.

To summarize, we present a study of the low-energy partial fluorescence yields ($5p\rightarrow 4d$, around 80 eV) for La when tuning the excitation energy through the deeper lying threshold ($3d\rightarrow 4f$, around 840 eV). We find that (1) a multitude of cascade transitions starting with $3d$ holes leads to a strong enhancement in $5p$-$4d$ fluorescence. By calculating the cascade-produced emission spectra via direct construction of de-excitation trees and then considering self-absorption, we find that (2) our model explains the qualitative behavior of the PFY and, in particular, agrees quantitatively with the measured contrast of the partial fluorescence yields.

Further, we find that (3) there are an increased number of $4d$ holes when the excitation energy is near the $3d$-$4f$ excitation thresholds. This conclusion is drawn from the significantly larger energy widths of the PFY spectra—and, therefore, larger integral $5p$-$4d$ fluorescence—of the experimental partial fluorescence yield curves, as compared to what is theoretically expected.

ACKNOWLEDGMENTS

The National Sciences and Engineering Research Council (NSERC), the Saskatchewan Synchrotron Institute, the NATO Expert Visit II program and the Research council of the President of the Russian Federation (Project No. NSH-1026.2003.2) supported this work. A. Moewes is a Canada Research Chair. The Advanced Light Source at Lawrence Berkeley National Laboratory is supported by the U.S. Department of Energy (Contract No. DE-AC03-76SF00098).

[1] *Soft X-Ray Emission Spectroscopy*, edited by J. Nordgren and E. Z. Kurmaev [J. Electron Spectrosc. Relat. Phenom. **110–111**, 1–363 (2000)].
[2] A. Kotani and S. Shin, Rev. Mod. Phys. **73**, 203 (2001).
[3] Stefan Brühl, Ph.D. thesis, University of Hamburg, Hamburg 1996.
[4] E. T. Verkhovtseva and P. S. Pogrebnjak, J. Phys. B **13**, 3535 (1980).
[5] E. T. Verkhovtseva, E. V. Gnatchenko, P. S. Pogrebnjak, and A. A. Tkachenko, J. Phys. B **19**, 2089 (1986).
[6] M. O. Krause, T. A. Carlson, and A. Fahlman, Phys. Rev. A **30**, 1316 (1984).
[7] L. J. Garvin, E. R. Brown, S. L. Carter, and H. P. Kelly, J. Phys. B **16**, L269 (1983).
[8] E. Arenholz, A. W. Kay, C. S. Fadley, M. M. Grush, T. A. Callcott, D. L. Ederer, C. Heske, and Z. Hussain, Phys. Rev. B **61**, 7183 (2000).
[9] A. Moewes, E. Z. Kurmaev, and D. L. Ederer, and T. A. Callcott, Phys. Rev. B **62**, 15 427 (2000).
[10] D. Nordlund, M. G. Garnier, N. Witkowski, R. Denecke, A. Nilsson, M. Nagasono, N. Mårtensson, and A. Föhlisch, Phys. Rev. B **63**, R121402(R) (2001).
[11] A. W. Kay, F. J. Garcia de Abajo, S.-H. Yang, E. Arenholz, B. S. Mun, N. Mannella, Z. Hussain, M. A. Van Hove, and C. S. Fadley, Phys. Rev. B **63**, 115119 (2001).
[12] J. Sugar, Phys. Rev. A **6**, 1764 (1972).
[13] C. Bonnelle, R. C. Karnatak and J. Sugar, Phys. Rev. A **9**, 1920 (1974)
[14] G. Kaindl, G. Kalkowski, W. D. Brewer, B. Perscheid, and F. Holtzberg, J. Appl. Phys. **55**, 1910 (1984).
[15] B. T. Thole, G. van der Laan, J. C. Fuggle, G. A. Sawatzky, R. C. Karnatak, and J.-M. Esteva, Phys. Rev. B **32**, 5107 (1985).
[16] A. Moewes, A. V. Postnikov, E. Z. Kurmaev, M. M. Grush, and D. L. Ederer, Europhys. Lett. **49**, 665 (2000).
[17] J. J. Jia, T. A. Callcott, J. Yurkas, A. W. Ellis, F. J. Himpsel, M. G. Samant, G. Stöhr, D. L. Ederer, J. A. Carlisle, E. A. Hudson, L. J. Terminello. D. K. Shuh, and R. C. C. Perera, Rev. Sci. Instrum. **66**, 1394 (1995).
[18] M. O. Krause, M. L. Vestal, W. H. Johnston, and T. A. Carlson, Phys. Rev. **133**, A385 (1964).
[19] A. G. Kochur and V. L. Sukhorukov, J. Phys. B **29**, 3587 (1996).
[20] A. G. Kochur, V. L. Sukhorukov, A. I. Dudenko, and Ph. V. Demekhin, J. Phys. B **28**, 387 (1995).
[21] J. P. Connerade and R. C. Karnatak, J. Phys. F: Met. Phys. **11**, 1539 (1981).
[22] E. J. McGuire, Phys. Rev. A **5**, 1043 (1972).
[23] B. Sonntag, T. Nagata, Y. Sato, Y. Satow, A. Yagishita, and M. Yanagihara, J. Phys. B **17**, L55 (1984).
[24] B. L. Henke, E. M. Gullikson, and J. C. Davis, At. Data Nucl. Data Tables **54**, 181 (1993).
[25] R. D. Cowan, *The Theory of Atomic Structure and Spectra* (University of California Press, Berkeley, 1981).